Chapter 6

Exchange Coupled nanocomposite $Nd_2Fe_{14}B/\alpha$-Fe system

6.1. Introduction

Nanocomposite permanent magnetic materials consisting of a hard magnetic phase like $Nd_2Fe_{14}B$ and a soft magnetic phase like α-Fe exhibit higher theoretical energy products compared to those of pure $Nd_2Fe_{14}B$ permanent magnets due to exchange coupling between the two phases [1]. In the case of two phase nanocomposites like $Nd_2Fe_{14}B/\alpha$-Fe, for an effective exchange coupling, the phases should be homogeneous and the grain size of the soft phase should be smaller than twice the domain wall width of the hard magnetic phase [2, 3] which is around 10 nm for $Nd_2Fe_{14}B/\alpha$-Fe. Many studies have been carried out on this type of magnetic materials to understand the behaviour of exchange coupling with respect to grain size. It has been reported [4, 5] that the exchange coupling enhances the remanence ratio to a value above 0.5. Increasing the grain size results in the magnetization reversal which suppresses the exchange coupling as seen from δM studies [6]. However, the remanence enhancement can also arise due to the dipolar coupling and the nature of coupling can be identified through Henkel plots [7, 8].

The nanocomposite exchange coupled materials can be synthesized using the melt spinning technique and a proper control over grain size can be obtained by varying the process conditions such as cooling rate and melting temperature. By varying the composition and wheel speed, either amorphous or crystalline ribbons can be produced. The amorphous ribbons can be crystallized using a suitable heat treatment to obtain the desired grain size. On the other hand the grain size of the ribbons, crystallized in the as-spun state itself, can be varied by controlling the wheel speed during melt spinning or by a post annealing step. The α-Fe soft phase appears for less than nearly 11 at.% of Nd for a fixed boron concentration of 6 at.% in $Nd_xFe_{94-x}B_6$ which is required for the synthesis of exchange coupled $Nd_2Fe_{14}B/\alpha$-Fe [9]. Very low concentrations of around 5.5 at.% Nd would result in the formation of Fe_3B which has a lower saturation magnetization than α-Fe [10]. Micromagnetic calculations have shown that the reduction of the magnetocrystalline

anisotropy in the grain boundary region would result in a reduced coercivity and enhanced exchange interaction [11]. In the as-spun ribbons, the effective anisotropy is high due to the non-uniform distribution of strains and imperfections in the grain boundary. Annealing would reduce the strains and imperfections in the grain boundary and hence will lower the magnetic anisotropy, which will lead to a better exchange coupling between the adjacent phases. The motivation of the present work is to understand the effect of grain boundary anisotropy on the exchange coupling mechanism in these materials.

6.2. Experiment

The ingots of the composition $Nd_{10}Fe_{85}B_5$ and $Nd_{11}Fe_{80}B_9$ were prepared by induction-melting the constituent elements with purity greater than 99 %, in the required weight proportions, several times in an evacuated quartz tube to ensure homogeneity. In order to compensate for the loss of Nd during evaporation an extra 1 at. % Nd was taken. The samples were weighed after the formation of ingot to check the loss of weight and it was found to be less than 0.5 %. The ingot thus prepared was melt-spun in a rotating copper wheel at a speed of 40 m/s in argon atmosphere. The resulting ribbons had a thickness of 18 μm and a width of 0.7 mm. The ribbons were annealed at various temperatures in an evacuated quartz tube with a pressure of 10^{-6} Torr. The X-ray diffraction measurements using Rigaku X-ray diffractometer with Cu-K_α radiation were carried out to identify the phases present in the ribbons. Since the XRD pattern of $Nd_2Fe_{14}B$ has more than a hundred reflections between the two theta values of 25 and 70 degree, the prominent peaks alone are indexed. The magnetic measurements were performed using a vibrating sample magnetometer (Tamakawa, Japan, Model VSM1230) at various temperatures above 300 K in a maximum magnetic field of 1.2 T applied parallel to the length of the ribbons. The demagnetization effect is negligible due to the large length to breadth ratio of the ribbons. For δM measurements, the samples were demagnetized first using an alternating magnetic field.

6.3. Results and Discussion

6.3.1. X-ray diffraction studies

The as-spun ribbons of the composition $Nd_{11}Fe_{80}B_9$ are amorphous with a broad hump in the XRD peak as shown in Fig. 6.1.(a). The ribbons annealed at 1023 K for 1 h

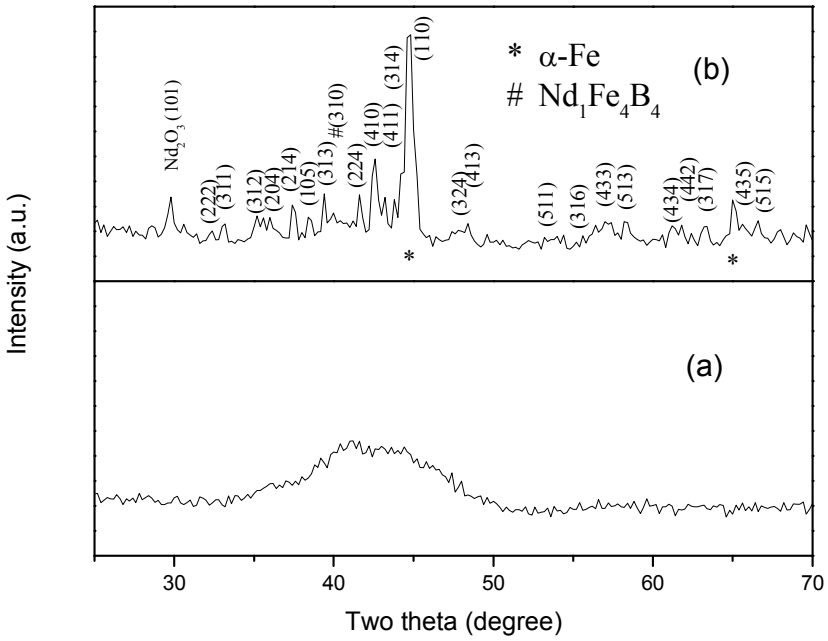

Fig. 6.1. The XRD pattern of the $Nd_{11}Fe_{80}B_9$ ribbon **(a)** as-spun and **(b)** annealed at 1023 K for 1 h.

showed a crystalline behaviour with $Nd_2Fe_{14}B$ and α-Fe phases as shown in Fig. 6.1.(b). The presence of some amount of Nd_2O_3 and metastable $Nd_1Fe_4B_4$ phases is also observed. The metastable $Nd_1Fe_4B_4$ phase arises due to higher boron concentration which follows from $Nd_{11}Fe_{80}B_9 \rightarrow 5Nd_2Fe_{14}B + 6Fe + Nd_1Fe_4B_4$. The grain size of the α-Fe phase is 38 nm whereas the $Nd_2Fe_{14}B$ phase has a grain size of 32 nm. The higher crystallization temperature for higher B concentration arises due to the enhanced thermal stability of amorphous Nd-Fe-B alloys as the viscosity of the alloy increases and hence the diffusion coefficient decreases [12] with B concentration. The as-spun $Nd_{10}Fe_{85}B_5$ ribbons are crystalline containing $Nd_2Fe_{14}B$ and α-Fe phases as shown in Fig. 6.2.(a). The ribbons are annealed at various temperatures at 793, 893 and 993 K to study the effect of grain size on the exchange coupling. The $Nd_2Fe_{14}B$ and α-Fe phases evolve from the composition $Nd_{10}Fe_{85}B_5$. The (314) peak of the $Nd_2Fe_{14}B$ phase is separated from the most intense peak (110) of α-Fe as the line width becomes narrower due to grain growth for the annealed ribbons as seen from Fig. 6.2(c) and (d). The grain sizes of the $Nd_2Fe_{14}B$ phase for both the as-spun $Nd_{10}Fe_{85}B_5$ ribbons and those annealed at 893 K are found to be around 36 nm. A slow scan XRD in the region of the most intense peak of α-Fe phase and fitting the same

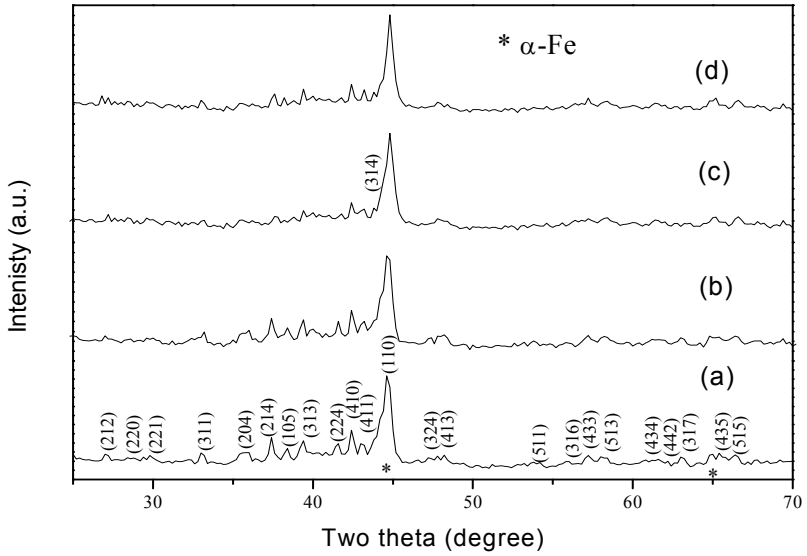

Fig. 6.2. The XRD pattern of the $Nd_{10}Fe_{85}B_5$ ribbons **(a)** as-spun, **(b)** annealed at 793 K and **(c)** 893 K and **(d)** 993 K for 20 min (* denotes α-Fe).

with a Lorentzian - shape gave a crystallite size of 30 nm for α-Fe in the as-spun state and 34 nm and 40 nm for the ribbons annealed at 893 K and 993 K respectively. From the XRD studies it is clear that a higher boron content induces amorphisation in the Nd-Fe-B ribbons. In such cases the crystalline phases $Nd_2Fe_{14}B$ and α-Fe are obtained by crystallizing the amorphous $Nd_{11}Fe_{80}B_9$ ribbons. Since the crystallization temperature (1023 K) is high, the grain sizes obtained are very large and, therefore, it is difficult to have exchange coupling between the two phases. Hence the $Nd_{10}Fe_{85}B_5$ composition, with which the two phases are obtained in the crystalline form with small crystal sizes in the as-spun state itself, is suitable for the fabrication of exchange coupled magnets.

6.3.2. Magnetization studies

6.3.2.1. Coercivity and remanence ratio

Figure 6.3 shows the magnetic hysteresis loop at 300 K and 373 K for the as-spun $Nd_{10}Fe_{85}B_5$ ribbons with an enhanced remanence ratio compared to that of the Stoner-Wohlfarth particles [13]. The enhanced remanence ratio may be due to exchange or magnetostatic interactions. The as-spun $Nd_{10}Fe_{85}B_5$ does not show a kink in the hysteresis loop measured at 300 and 373 K. But the $Nd_{11}Fe_{80}B_9$ ribbon annealed at 1023 K and the

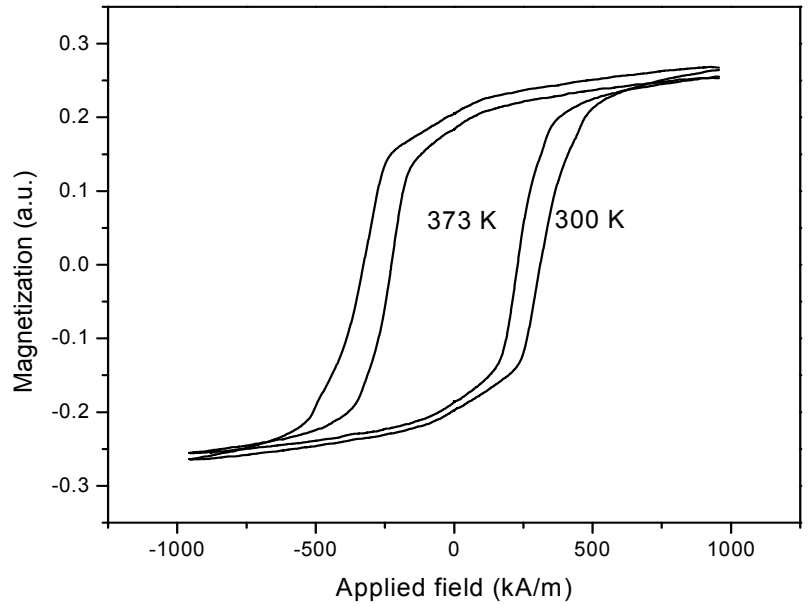

Fig. 6.3. The hysteresis loop of the as-spun $Nd_{10}Fe_{85}B_5$ ribbons at 300 K and 373 K.

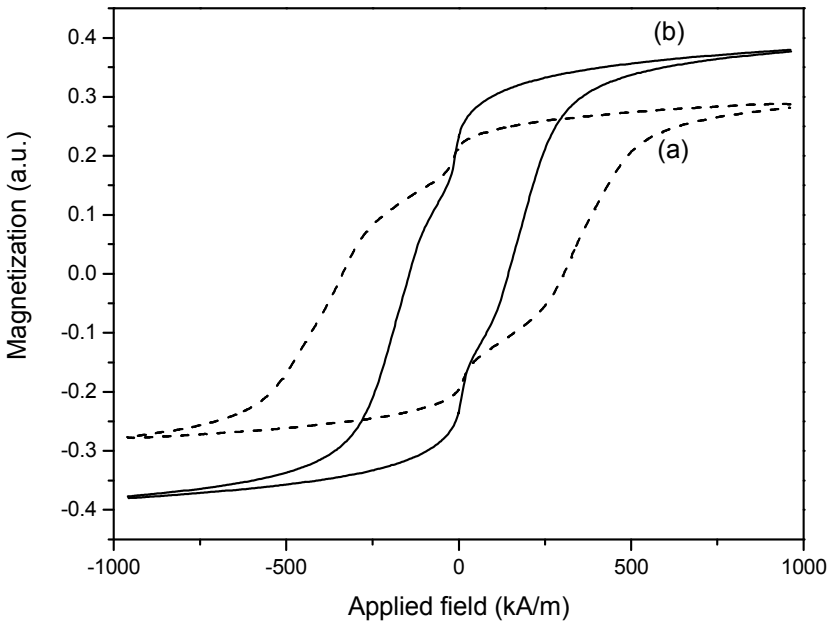

Fig. 6.4. The hysteresis loop at 300 K of (a) $Nd_{11}Fe_{80}B_9$ annealed at 1023 K and (b) $Nd_{10}Fe_{85}B_5$ annealed at 993 K.

$Nd_{10}Fe_{85}B_5$ ribbon annealed at 993 K show a kink in the hysteresis loop at 300 K as shown in Figs. 6.4(a) and (b) respectively. The kink in the hysteresis loop indicates that the $Nd_2Fe_{14}B$ and α-Fe phases are not exchange coupled. In the case of $Nd_{11}Fe_{80}B_9$ ribbons annealed at 1023 K, the exchange coupling is hindered by the presence of $Nd_1Fe_4B_4$ and the Nd_2O_3 phases and also by the large grain size of 38 nm for α-Fe resulting in a kink in the hysteresis loop. Similarly a kink in the hysteresis loop is visible for the $Nd_{10}Fe_{85}B_5$ composition annealed at 993 K because of the large grain size of 40 nm for α-Fe phase in accordance with the theoretical calculations [3]. The low coercivity of the $Nd_{10}Fe_{85}B_5$ ribbons is because of the large α-Fe phase content at low Nd concentrations as reported by Davies [9]. Figure 6.5 shows the coercivity and remanence ratio of the as-spun and annealed $Nd_{10}Fe_{85}B_5$ ribbons at various temperatures. It is seen that the annealed ribbons show lower coercivity when compared to that of the as-spun ribbons. Ramesh [14] have shown that quenching induces stress anisotropy which increases the coercivity. Studies by de Groot and Kort have shown that stress and strain are present in the grain boundary of $Nd_2Fe_{14}B$ which could affect the coercivity [15]. Since the exchange coupling between the $Nd_2Fe_{14}B$ and α-Fe phases is mediated through the grain boundary, the stress and strain present in the grain boundaries will influence the coercivity. Hence, the reduction in the coercivity of the annealed ribbons is due to the decrease in the effective anisotropy on annealing which in turn will enhance the exchange coupling. The decrease in coercivity with temperature is due to the decrease in anisotropy with temperature [16]. Since the Curie temperature of the $Nd_2Fe_{14}B$ phase is 585 K, the coercivity drops from a few hundreds to a few tens of kA/m when the temperature approaches 600 K. For the Stoner-Wohlfarth particles the remanence ratio (M_r/M_s) is always less than 0.5

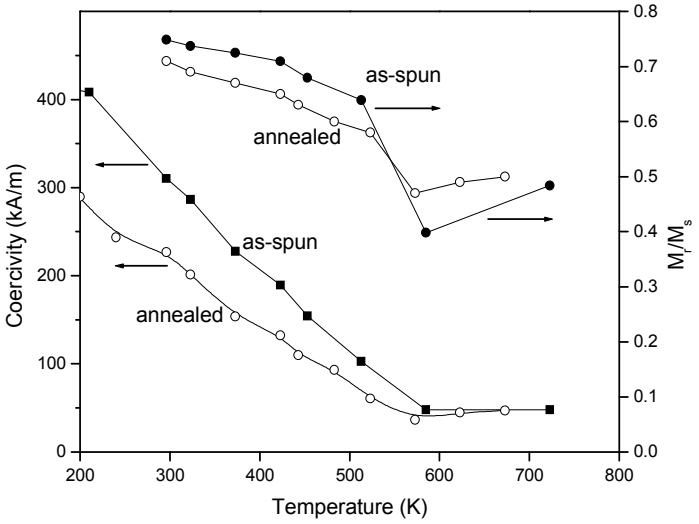

Fig. 6.5. The coercivity and remanence ratio of the as-spun and annealed $Nd_{10}Fe_{85}B_5$ ribbons at various temperatures.

[13]. In our case, the enhancement in the remanence ratio even up to 530 K which is close to the Curie temperature of the $Nd_2Fe_{14}B$ phase, indicates that there is a coupling between the grains. The remanence ratio is higher for the as-spun ribbons than for the annealed ribbons as shown in Fig. 6.5. The enhanced remanence ratio indicates the presence of either the exchange or the magnetostatic interactions or both [17-19]. Hence the annealed ribbons, show a smaller remanence ratio compared to that of the as-spun ribbons. because of the reduction in the magnetostatic (dipolar) interaction due to annealing, as verified from the δM measurements discussed in Section 6.3.2.1. Since both exchange and dipolar couplings will give rise to an enhanced remanence ratio, we have carried out δM studies to identify the type of coupling.

6.3.2.1. The δM studies

The δM measurements were performed at 300 K and also at high temperatures but below the Curie temperature of the $Nd_2Fe_{14}B$ phase for the as-spun and the 893 K annealed ribbons of $Nd_{10}Fe_{85}B_5$. The δM values are calculated from the Isothermal Remanence Magnetization (IRM) measurements, which is done by plotting the remanent magnetization as a function of field from a demagnetized sample and from Direct Current Demagnetization (DCD) measurements by applying a reverse field and measuring the remanence of the sample.

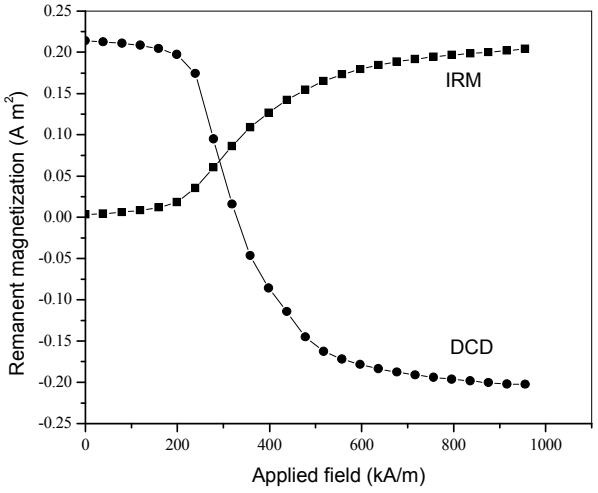

Fig. 6.6. The plot of IRM and DCD curves for the as-spun ribbons of $Nd_{10}Fe_{85}B_5$ at 300 K.

One such IRM and DCD plot for the as-spun ribbons at 300 K is shown in Fig. 6.6. The δM value is calculated using the relation [8]

$$\delta M = \frac{\{M_D(H) - [M_r(H_{\max}) - 2M_R(H)]\}}{M_r(H_{\max})} \tag{6.1}$$

where $M_D(H)$ is the DCD remanence, $M_R(H)$ is the IRM and $M_r(H_{max})$ is the saturation remanence. A positive value for δM represents exchange interaction and a negative value

denotes dipolar interaction between the crystals. Figure 6.7 shows the *δM* plot of the $Nd_{10}Fe_{85}B_5$ ribbons at 220 K, 300 K, 323 K and 373 K for the as-spun and for the ribbons annealed at 893 K. The as-spun ribbons show dipolar coupling at 220 K, both exchange and dipolar couplings at 300 and 323 K, a stronger exchange coupling at 323 K than at 300 K and only dipolar coupling at 373 K whereas the annealed ribbons show exchange coupling alone at 300 and 323 K and only dipolar coupling at 220 and 373 K.

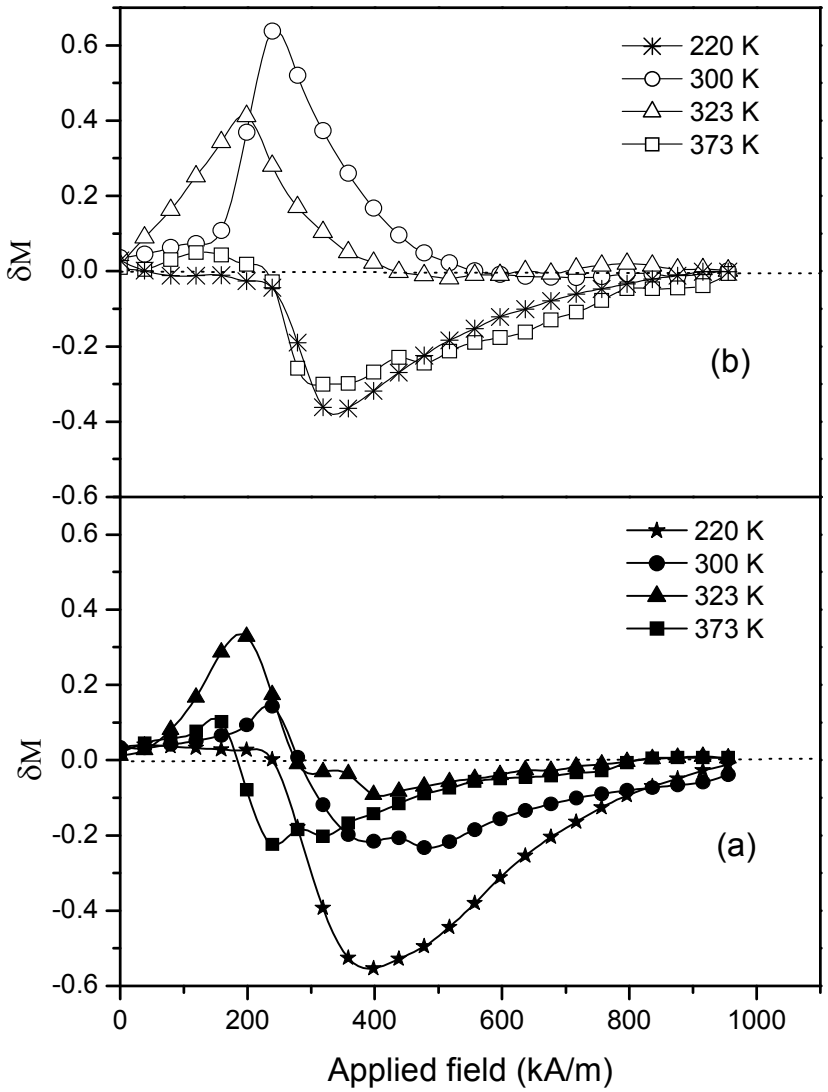

Fig. 6.7. The δM plot at various temperatures for **(a)** as-spun and **(b)** annealed $Nd_{10}Fe_{85}B_5$.

6.3.2.1 (a) Dipolar and exchange couplings in annealed ribbons

The δM plot at various temperatures for the $Nd_{10}Fe_{85}B_5$ ribbons annealed at 893 K is shown in Fig. 6.7.(b). The annealed ribbons show dipolar coupling at 220 K as seen from the negative value of the δM peak shown in the figure. The domain wall width, δ_W is given by

$$\delta_W = \pi\sqrt{(A/K)} \tag{6.2}$$

where A is the exchange stiffness and K is the anisotropy constant of the hard magnetic phase. The domain wall width is proportional to the exchange length, l_{ex} given by

$$l_{ex} = \sqrt{\frac{A}{K}} \tag{6.3}$$

which depends on the exchange stiffness and the anisotropy constant. In $Nd_2Fe_{14}B$, the magnetocrystalline anisotropy is dominant because of the spin-orbit coupling [15]. Since K is more sensitive to temperature than A [16], the former has a stronger influence on the temperature dependence of δ_w. The magnetic anisotropy constant K is a sum of K_1+K_2, where K_1 and K_2 are the first and second magnetocrystalline anisotropy constants respectively. In $Nd_2Fe_{14}B$, K is large in magnitude due to a significant contribution from K_2 at temperatures below 300 K [20]. Hence δ_W is small and exchange interaction is weak in this temperature range and only dipolar interaction is present.

At 300 K an enhancement in the exchange coupling is observed in the annealed ribbons. Since K_2 is negligible and K is reduced in magnitude at 300 K and since the decrease in A at this temperature can be only very small, the exchange length increases and hence the exchange coupling is strengthened.

We also observe a reduction in the exchange coupling at 323 K for the annealed ribbons and only dipolar coupling at 373 K. Above 300 K the anisotropy constant K_2 is negligible and only K_1 alone contributes to K. The exchange stiffness is related to the saturation magnetization, J_s by [21]

$$A = cJ_s^2 \tag{6.4}$$

The anisotropy K decreases only linearly with temperature above 300 K whereas the exchange constant A decreases rapidly, as it depends on the square of the saturation

magnetization which decreases rapidly above 300 K [15,20] as the Curie temperature of the $Nd_2Fe_{14}B$ phase is only 585 K. Hence the exchange length is reduced and as a consequence a reduction in the strength of exchange coupling is observed at 323 K. At 373 K the reduction in A should be very large so that the exchange coupling vanishes and hence only dipolar coupling is observed.

6.3.2.1 (b) Dipolar and exchange couplings in as-spun ribbons

The δM plot at various temperatures for the as-spun $Nd_{10}Fe_{85}B_5$ ribbons are shown in Fig. 6.7.(a). We observe only dipolar coupling at 220 K for the as-spun ribbons. The presence of only dipolar coupling at 220 K is due to the large value of the anisotropy constant K as discussed in the previous section.

When the measurement temperature increases to 300 K both exchange and dipolar couplings are present in the as-spun ribbons. The presence of exchange coupling at 300 K is due to the expected faster decrease in the value of K with temperature compared to the temperature dependence of A which results in an increase in the value of l_{ex} as discussed earlier.

At 300 K we observe only the exchange coupling in the annealed ribbons whereas both exchange and dipolar couplings are present in the as-spun ribbons. It is well known in the literature that the reduction in grain size will enhance the exchange coupling between the two phases [1-5]. Eventhough the grain size of the as-spun ribbons is smaller than that of the annealed ribbons by 4 nm we observe dipolar coupling and a reduction in the exchange coupling for the as-spun ribbons. Since the exchange coupling is a result of short-range interaction, the interaction between adjacent grains is possible only if there are no barriers which separate them. In nanocomposites comprising of soft and hard magnetic phases, the exchange coupling between the adjacent grains of the two phases can take place without affecting the coercivity whenever (i) they are not isolated by a non-magnetic or paramagnetic phase, (ii) the grain size of the soft magnetic phase is less than twice the domain wall thickness of the hard magnetic phase, which is 10 nm and (iii) the two phases are homogeneously distributed [1-5,22,23]. However, if there is a barrier, for example, the grain boundary, which separates the two phases, the anisotropy at the grain boundary will be higher than that in the bulk grain due to the strains induced in the grain boundary. The

grain boundary anisotropy weakens the exchange interaction. Theoretical calculations by MacLaren and Willoughby also predict that the presence of grain boundary component should reduce the intergrain exchange coupling [24]. Thus a relatively weaker exchange coupling between the soft and hard magnetic phases, inspite of the smaller grain size in the as-spun ribbons, indicates the presence of grain boundary anisotropy in the as-spun ribbons.

The δM measurements at 323 K show an enhanced exchange coupling compared to that at 300 K for the as-spun ribbons. A faster reduction in the value of K at this temperature compared to that of A should have caused an increase in the exchange length and strengthened the exchange interaction.

6.3.2.2. The Henkel plot

Figure 6.8 shows the Henkel plot of the as-spun and annealed ribbons at various temperatures along with Stoner-Wohlfarth behaviour represented by the diagonal line. The

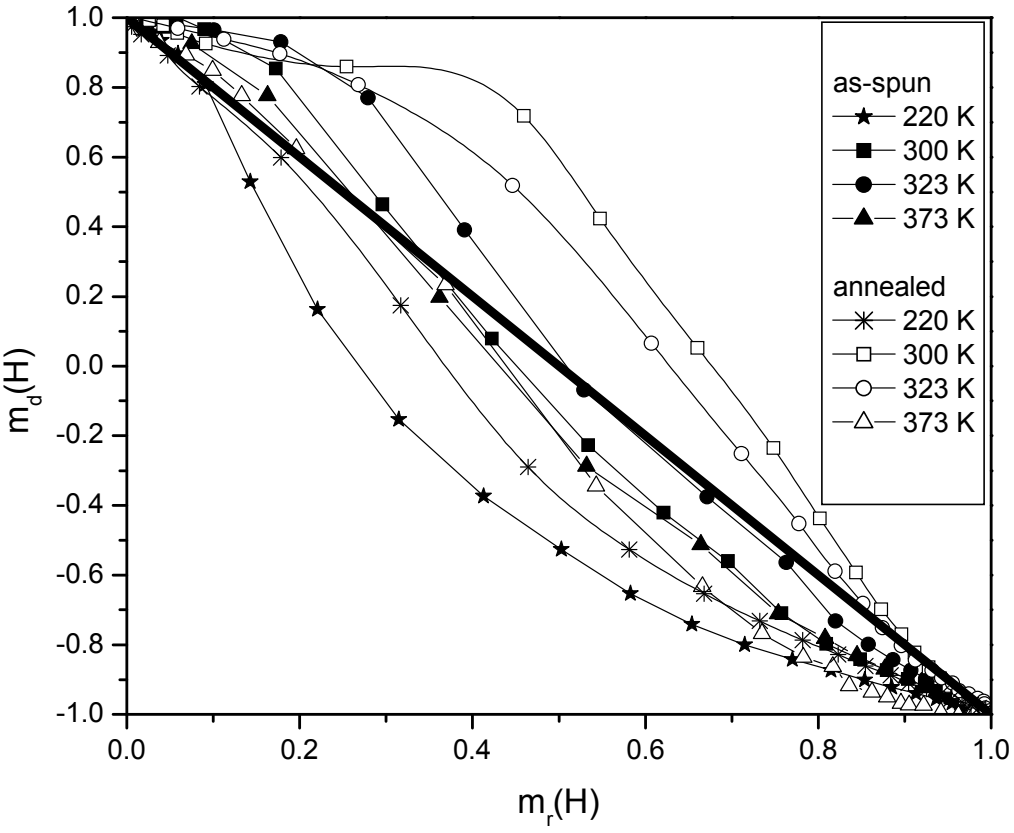

Fig. 6.8. The Henkel plot of the $Nd_{10}Fe_{85}B_5$ at various temperatures for the as-spun and for the ribbons annealed at 893 K. (The diagonal line represents Stoner-Wohlfarth behaviour).

Henkel plot of $m_d(H)$ vs. $m_r(H)$, where $m_d(H) = M_D(H)/ M_r(H_{max})$ and $m_r(H) = M_R(H)/M_r(H_{max})$ represents the type of interaction (exchange or dipolar) present in the system. Exchange and dipolar interactions are shown by the shift of the curve to above and below the diagonal line respectively. From the figure it is seen that in the as-spun and annealed samples, when the temperature is increased from 220 K towards 323 K, the dipolar coupling decreases which again increases at 373 K. The increase in dipolar coupling when the temperature is decreased from 323 to 220 K is due to the higher magnetocrystalline anisotropy constant of the hard magnetic phase which results in the weakening of the exchange interaction. The increase in the dipolar interaction at 373 K is due to the reduction in the exchange constant *A* with temperature. From the Henkel plot, it is also seen that the short-range exchange interaction is weakened whenever the magnetocrystalline anisotropy constant increases or the exchange constant decreases as discussed in the earlier sections.

6.3.2.3. The χ_{irr} plot

The irreversible susceptibility $\chi_{irr} = dM_d(H)/dH$ represents the strength of the interactions between the grains. A single peak in the χ_{irr} vs. reverse applied magnetic field plot represents a well coupled system and the presence of two peaks corresponds to two magnetic phases with a weak coupling between them [26]. Figure 6.9 (a) shows the plot of χ_{irr} as a function of field for the as-spun samples at 300, 323 and 373 K and the inset shows the plot at 220 K. Figure 6.9 (b) shows a similar plot for the annealed ribbons measured at 300 and 323 K and the inset shows the measurement at 220 K. For the as-spun ribbons, the appearance of two broad peaks is due to the fact that the nucleation field is different for differently oriented grains [26] and this indicates a weak coupling between the two phases. The peak shifts towards low fields with increasing temperature due to the reduced magnetocrystalline anisotropy and increased exchange coupling. The peak at a higher field represents a large distribution in the nucleation fields and it is found to be 438 kA/m at 300 K for the as-spun ribbons which decreases to 278 kA/m at 373 K. The annealed ribbons show only a single peak. For the annealed ribbons, the peak due to the distribution in nucleation fields is not distinctly seen as there is a strong exchange coupling which decreases the nucleation field and hence the corresponding peak merges with the Gaussian

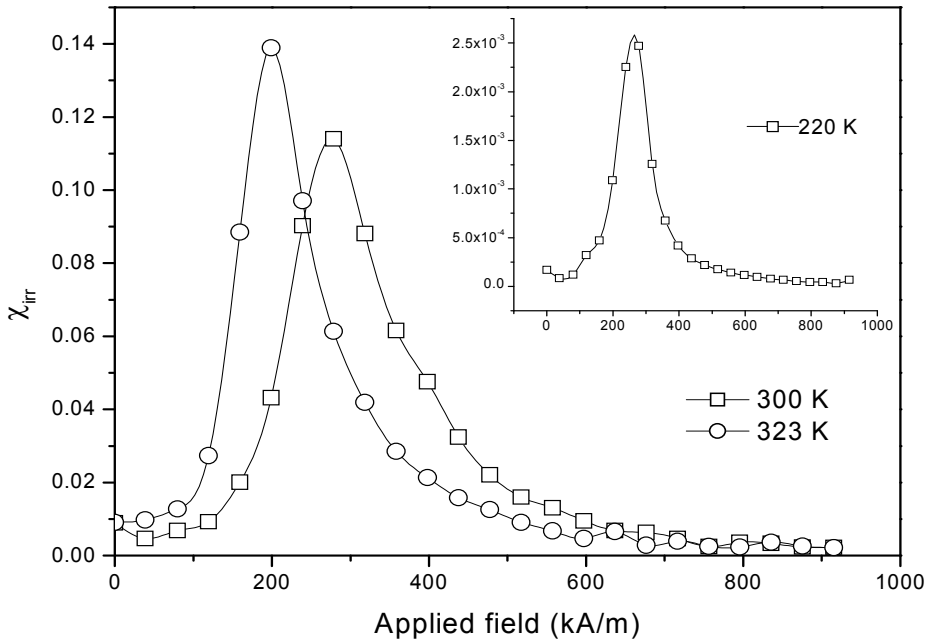

Fig. 6.9 (b) The irreversible susceptibility in a reverse applied field for the annealed $Nd_{10}Fe_{85}B_5$ ribbons at various temperatures (Inset shows the irreversible susceptibility of the same ribbons at 220 K).

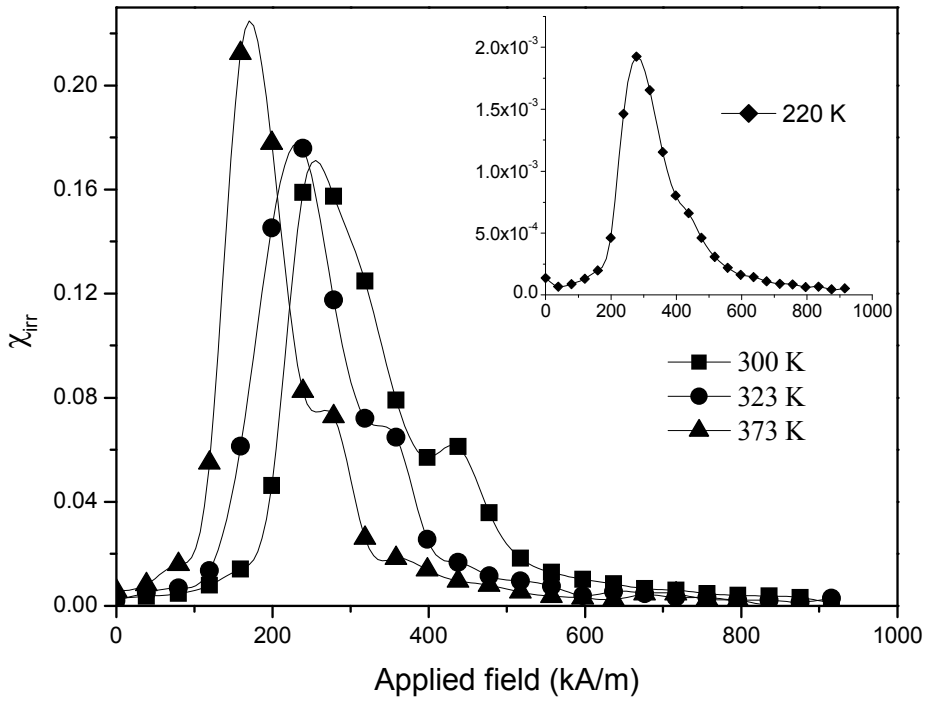

Fig. 6.9 (a) The irreversible susceptibility in a reverse applied field for the as-spun $Nd_{10}Fe_{85}B_5$ ribbons at various temperatures (Inset shows the irreversible susceptibility of the ribbons at 220 K).

peak representing exchange interactions, as shown in the inset of Fig. 6.9.(b). The χ_{irr} plot at 220 K for the annealed ribbons, as shown in the inset of Fig. 6.9.(b), is narrower compared to that of the as-spun samples suggesting that there is no distribution in the nucleation fields. Thus it is seen from the δM plots that the exchange interaction is enhanced in the annealed ribbons due to the reduction of effective magnetic anisotropy. This suggests that the exchange coupling becomes stronger if the nanocomposite ribbons are free from grain boundary anisotropy.

6.4. Conclusion

The exchange coupling between $Nd_2Fe_{14}B$/α-Fe phases is present when the grain size of the α-Fe phase is less than 34 nm. Due to the presence of grain boundary anisotropy, the as-spun nanocomposite ribbons show exchange and dipolar couplings. Annealing removes the strains and defects introduced in the grain boundaries and reduces the grain boundary anisotropy, which results in an increase in the strength of the exchange coupling. Very high energy products can, therefore, be achieved by removing the grain boundary anisotropy.

References

[1] E. F. Kneller and R. Hawig, IEEE Trans. Magn. **MAG-27** (1991) 3588.

[2] R. Skomski and J. M. D. Coey, Phys. Rev. B **48** (1993) 15812.

[3] R. Fisher, T. Leineweber, and H. Kronmüller, Phys. Rev. B **57** (1998) 10723.

[4] W. Gong, G. C. Hadjipanayis, and R. I. Krause, J. Appl. Phys. **75** (1994) 6649.

[5] J. Bauer, M. Seeger, A. Zern, and H. Kronmüller, J. Appl. Phys. **80** (1996) 1667.

[6] Q. Chen, B. M. Ma, B. Lu, Q. Huan, and D. E. Laughlin, J. Appl. Phys. **85** (1999) 5917.

[7] J. Garcia-Otero, M. Porto, and J. Rivas, J. Appl. Phys. **87** (2000) 7376.

[8] P. E. Kelly, K. O'Grandy, P. I. Mayo, and R. W. Chantrell, IEEE Trans. Magn. **25** (1989) 3881.

[9] H. A. Davies, J. Magn. Magn. Mater. **157-158** (1996) 11.

[10] M. Uehara, S. Hirosawa, H. Kanekiyo, N. Sano, and T. Tomida, Nanostructured Mater. **10** (1998) 151.

[11] R. Fischer and H. Kronmüller, Phys. Rev. B **54** (1996) 7284

[12] B.-G. Shen, L.-Y Yang, H.-Q. Guo, and J.-G. Zhao, J. Appl. Phys. **75** (1994) 6312.

[13] E. C. Stoner and E. P. Wohlfarth, Phil. Trans. Royal Soc. London, Ser. A **240** (1948) 599.

[14] R. Ramesh, J. Appl. Phys. **68** (1990) 5772.

[15] C. H. de Groot and K. de Kort, J. Appl. Phys. **85** (1999) 8312.

[16] K. H. J. Buschow, Rep. Prog. Phys. **54** (1991) 1123.

[17] T. Schrefl, J. Fidler, and H. Kronmüller, Phys. Rev. B **49** (1994) 6100.

[18] T. Schrefl and J. Fidler, J. Magn. Magn. Mater. **177** (1998) 970.

[19] H. Qu and J. Y. Li, Phys. Rev. B **68** (2003) 212402.

[20] M. Sagawa, S. Hirosawa, H. Yamamoto, S. Fujimura, and Y. Matsuura, Jpn. J. Appl. Phys. **26** (1987) 785.

[21] R. Fisher and H. Kronmüller, Phys. stat. sol. (a). **166** (1998) 489.

[22] H. Kronmüller and T. Schrefl, J. Magn. Magn. Mater. **129** (1994) 66.

[23] Y. Gao, J. Zhu, Y. Weng, E. B. Park, and C. J. Yang, J. Magn. Magn. Mater. **191** (1999) 146.

[24] J. M. MacLaren and S. D. Willoughby, J. Appl. Phys. **89** (2001) 6895.

[25] H. Chiriac, M. Marinescu, P. Tiberto, and F. Vinai, Mater. Sci. Eng. A **304-306** (2001) 957.

[26] Z. Zhao, Q. F. Xiao, Z. D. Zhang, M. Dahlgren, R. Grössinger, K. H. J. Bushcow, and F. R. de Boer, Appl. Phys. Lett. **75** (1999) 2298.